2.2 Biomedical Simulation Models of Human Auditory Processes

Biomedical Simulation Models of Human Auditory Processes

Mehmet M.A. Bıçak, Ph.D
Adaptive Technologies Inc.
mehmet@adaptivetechinc.com

Abstract. Detailed acoustic engineering models that explore noise propagation mechanisms associated with noise attenuation and transmission paths created when using hearing protectors such as earplugs and headsets in high noise environments. Biomedical finite element (FE) models are developed based on volume Computed Tomography scan data which provides explicit external ear, ear canal, middle ear ossicular bones and cochlea geometry. Results from these studies have enabled a greater understanding of hearing protector to flesh dynamics as well as prioritizing noise propagation mechanisms. Prioritization of noise mechanisms can form an essential framework for exploration of new design principles and methods in both earplug and earcup applications. These models are currently being used in development of a novel hearing protection evaluation system that can provide experimentally correlated psychoacoustic noise attenuation. Moreover, these FE models can be used to simulate the effects of blast related impulse noise on human auditory mechanisms and brain tissue.

1 INTRODUCTION

Modeling the performance of hearing protection devices (HPDs), using numerical methods such as Finite Element (FE) Analysis techniques, is needed for further improving the noise attenuation performance of hearing protectors for personnel who work in high noise environments. A typical example for such environment is an aircraft carrier deck, where noise levels can range from 130 dB sound pressure level (SPL) to as high as 150 dB SPL due to exhaust gases emitted from aircraft engines. Wearing an effective HPD is critical in this acoustically dangerous environment to prevent permanent hearing loss. Conventional HPDs are designed to reduce the risk of hearing damage from acoustic energy transmitted to the eardrum through air conduction (AC) through the ear canal. However, the maximum level of hearing protection obtained by using a conventional HPD is limited due to the presence of flanking paths of energy transmission to the cochlea. This flanking energy transmission is referred to as "bone conduction" (BC). It is accepted that the majority of the transmitted energy via BC to the middle and inner ear components is through the cartilage, skin, soft tissue and fluids of the human head. The limit of hearing protection performance set by the BC pathways is commonly termed the "BC limit" in hearing protection literature [1].

There has been increased development of computer simulations in the area of auditory mechanics [2,3,4,5], which has been facilitated by the growing sophistication of hardware and software technology. These simulations allow researchers to explore complicated biomechanical systems, often times involving numerous components with intricate geometries, complicated non-linear material properties and challenging boundary conditions. FE simulation methods offer significant advantages over traditional experimental methods, partly due to the inability of experimental methods to effectively measure internal human head and auditory system response to acoustic excitation. In contrast, all relevant structural and acoustic information, such as mode shapes, displacements, pressures and energy flow (intensity), are accessible at any arbitrary location within the FE simulation. FE simulation also offers the ability to visualize and study the three-dimensional dynamic response of the system, allowing for the ability to gain significant insight into the dynamic system behavior. However, the usefulness of the FE simulation is largely dependent on the fidelity of the model representative of the physical system. Therefore, accurate and relevant experimental information is needed to support the development of FE simulations.

This study, the use of experimental data to develop a FE simulation of a human subject for the investigation of AC and BC pathways, as well as HPD to flesh dynamics, is presented in this paper.

2 AUDITORY PATHWAYS

Understanding AC and BC phenomena is critical in developing improved hearing protection devices (HPDs) for extremely high noise environments. However, its underlying mechanics, especially with respect to acoustically induced BC, are not sufficiently understood. This is in part due to the relative complexity in developing analytical and/or numerical models that accurately capture the interactions between the macro dynamics of the skull and the micro dynamics of the middle ear and cochlea. Figure 1 shows the components of the AC and BC pathways which include the pathways presented by Stenfelt [6] as well as the pathways due to the presence of an earplug.

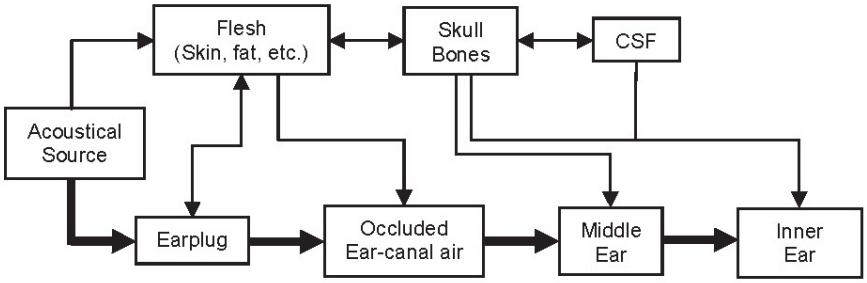

Figure 1. A model of acoustical pathways considering the occlusion due to the earplug. Occluded AC pathway is depicted by using thick lines.

When the external ear canal is effectively occluded by a high attenuation HPD, sound may not reach the cochlea through the direct acoustic excitation of the eardrum. In this case, sound energy may be transmitted to the middle-ear and the inner ear region via:

- Acoustically-induced skull vibration
- Transmission through nasal/oral cavities and the Eustachian tube to the middle ear
- Residual vibration of the earplug and canal bone-skin layer

Traditionally, most researchers in the BC field have focused on the skull vibration path (both rigid-body and flexural vibration) [7,8,9] because this is the most intuitive path of energy transmission to the auditory system, and because development of a BC exciter for medical purposes is often a research focus. Studies show that the average human skull *in vitro* exhibits the first resonant frequency at around 1 kHz [10]. Therefore, when subjected to external acoustic or structural excitation, a skull will exhibit dominant rigid-body vibrations (i.e. translation and rotation) at frequencies below about 1 kHz and flexural vibrations at frequencies above 1 kHz. In the current context of hearing protection, which involves an acoustic excitation rather than direct structural excitation, it is also possible that the other two paths described above may contribute to BC at certain limited frequency ranges.

Following the acoustic energy transmission through the skull to the auditory system, the main mechanisms involved in the excitation of the basilar membrane (BM) vibration in the cochlea are often categorized as follows:

- BC response of the middle ear
- BC response of the inner ear

Although separating the BC mechanisms into these two categories for simplification has been customarily done in literature, it should be noted that the mechanics of the middle ear and the inner ear are inter-related and one cannot completely treat them as independent.

3 DEVELOPMENT OF FE MODEL

To achieve the goal of developing a FE model which is capable of simulating AC and BC sound transmission, it is important to investigate human anatomical features

separately. It is impractical to model all the physiological features present in the actual physical system. Therefore, a certain degree of simplification has to be carried out, selecting only the essential features of the actual physical system for modeling based on *a priori* knowledge.

The high-fidelity FE models of the auditory system, including the relevant HPD, should be created using accurate geometrical information obtained from 3D imaging data. However, only skull, outer ear, ear-canal and the locations of middle ear bones can be extracted using a volume computed tomography (CT) scanning due to current limitations of spatial resolution from the lower exposure levels. In order to obtain highly detailed geometrical information, microCT scanning may be employed. However, this method is only applicable to cadavers due to intense dose levels at the human head. Due to this issue, FE model middle ear and cochlea geometries of a specific subject are usually based on cadaver scanned geometry. The developed FE models of the skull and outer-ear from CT scans as well as the isolated middle-ear and cochlea FE model based on microCT scans should be integrated to form a complete geometrical part of the whole auditory system model. An example of this process is presented for the middle-ear and cochlea in Figure 2 and 3.

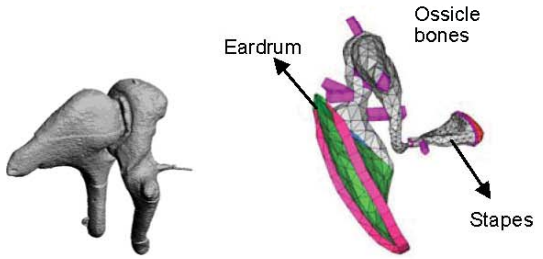

Figure 2. 3D solid model of malleus and incus derived from microCT imaging data (left), middle-ear FE model (right).

The integration of these two FE models with a developed skull model will result in having the complete FE model which is shown in Figure 4.

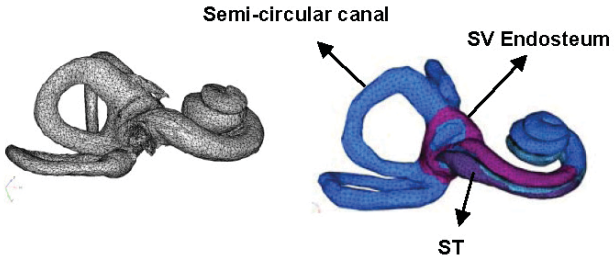

Figure 3. 3D solid model of cochlea derived from microCT imaging data (left), FE cochlear model with SV[1] endosteum and ST[2] (right). (Not to scale)

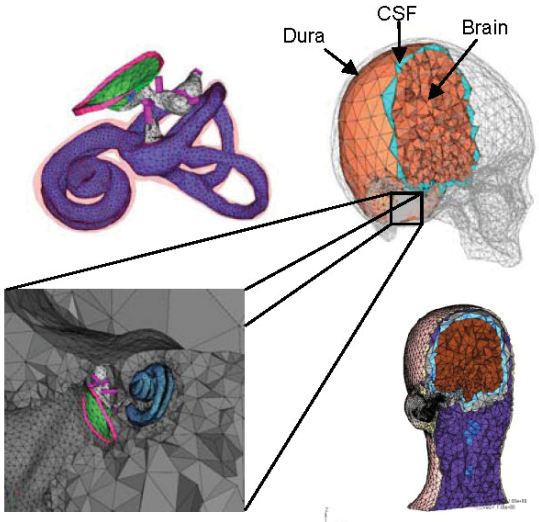

Figure 4. Integrated FE models, cochlea-middle ear (topleft), outer-ear skull including cochlea-middle ear FE (topright) and whole head FE model (bottomright).

4 NUMERICAL RESULTS AND VALIDATION

Material properties of various components should be selected by consulting the data provided in existing references on auditory system FE modeling [2,3,11,12]. The past literature reveals that large uncertainty still exists regarding the values of material properties for auditory system components. In past auditory system FE modeling efforts, material property values were typically determined by iteratively adjusting the literature values until good correlation was obtained between simulated and experimental dynamic response data [13]. This approach is adapted for the current FE

[1] Scala Vestibuli
[2] Scale Tympani

model in this study; the different material property values presented in literature are iteratively updated until agreement was obtained between published experimental data of dynamic component response and FE model results.

4.1 Simplification of circum/intra-aural flesh

One important simplification of the FE model is to use a single isotropic material for modeling the internal physiological structure of the human circum/intra-aural flesh (which includes the ear cartilage, fat, muscle and skin) rather than modeling the components individually. The validity of this assumption is investigated by comparing two FE models. One model is a realistic multi-component flesh model that contains the individually modeled internal structural components, while the second model is a homogenized flesh model, where the flesh is assumed to consist entirely of one type of material.

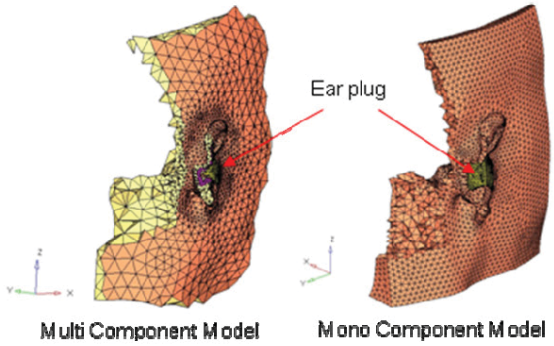

Figure 5. Multi-component vs. homogenized circum/intra-aural FE models.

Figure 5 shows images of these two models. Figure 6 shows the simulated insertion loss results for the multi-component model versus the homogenized flesh model results, along with experimental data. Four separate cases for the homogenized model are created with differing values for the flesh material elastic modulus; the values are increased by a factor of 1, 1.5, 2 and 3. It is observed from Figure 6 that the insertion loss for the case with a homogenized flesh, with the modulus increased by a factor of 2 from the baseline, shows good agreement with the baseline multi-component model. This suggests that the flesh model can be simplified into a single material structure with an effective elastic modulus, to ultimately reduce model complexity.

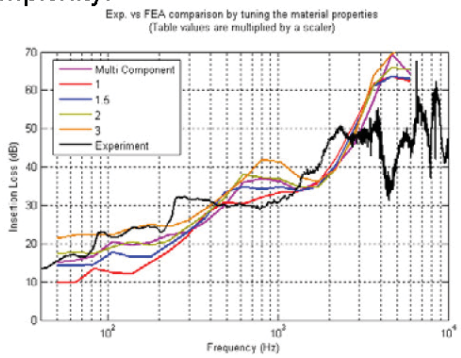

Figure 6. FE-simulated earplug attenuations (insertion loss) for the multi-component and homogenized circum/intra-aural flesh model. The Young's modulus of the flesh material for the homogenized flesh model was increased by a factor of 1, 1.5, 2 and 3.

4.2 Skull model

Mechanical response of the skull FE model with cranial content is compared against published experimental data [10,14]. The current skull model results with cranial content are in agreement with experimental data of point mechanical impedance at a location around mastoid, as shown in Figure 7. Figure 8 shows acceleration at contra- and ipsi-lateral cochlea locations in response to a force input at the mastoid location.

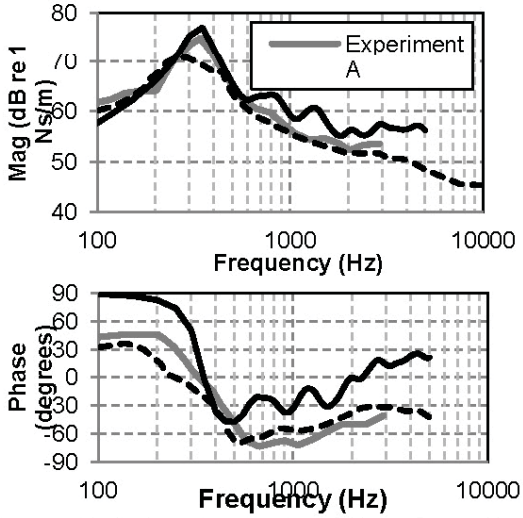

Figure 7. FE and experimental point mechanical impedance response for a skull with the cranial content.

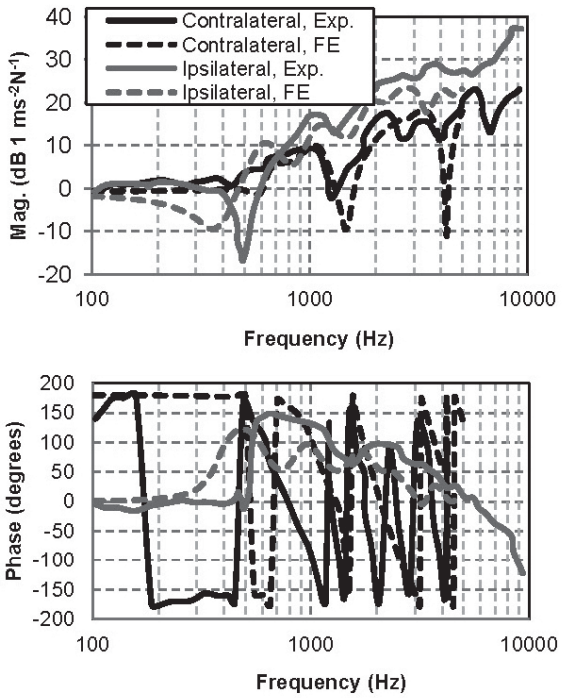

Figure 8. FE and experimental ipsilateral and contralateral accelerance response for a skull with the cranial content.

4.3 Middle-ear and Cochlea models

The FE model material properties and mesh characteristics of the middle-ear were discussed previously in Homma et al. [15]. The BM, which is determined to be the most significant component in the cochlea, is developed with orthotropic material properties. Detailed mechanical property and geometry of the BM were also described in the final report for an Air Force STTR program, topic number AF06-T035 [13]. To combine the middle-ear and the cochlear models, the stapes is attached to the cochlea via the stapes annular ligament, while the nodes along the perimeter of the stapes annular ligament are fixed to the cochlear bony shell. The current middle ear FE model does not include the air volumes associated with the middle ear cavity and the ear canal, primarily because the loading effects due to the air volumes are not considered to be significant under normal conditions. However, when air volumes are made significantly small by deep-occlusion of the ear canal or by a significant reduction in middle ear cavity volume, it is possible that the reduced air volume could provide additional stiffness to the middle ear system, therefore altering the system response characteristics. If this proves relevant, then it is likely that air volumes must be included in FE models. However, the reference experimental data of the middle ear, in both AC and BC conditions, are obtained without significant air loading, therefore this assumption is likely to be valid.

Model parameters are adjusted so that the FE model exhibits the correct impedance of the stapes/cochlea system with the fluid-filled cochlea, as well as with the cochlear fluid removed. Figure 9 shows that the impedance contribution from the cochlea itself is mostly resistive, which is evident from the increased damping effect around the system resonance at 3-4 kHz.

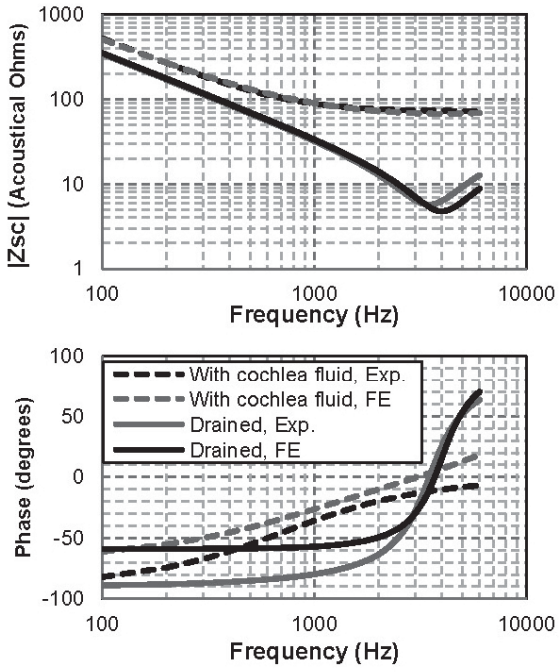

Figure 9. Input acoustic impedance (pressure / velocity) of cochlea/stapes system, z_{sc}: matching FE model response against target response data [16].

The middle-ear pressure gain function, which is defined as the ratio of oval window pressure (P_{OW}), to ear-canal pressure (P_{EC}), is another useful metric for FE model

validation, and is shown in Figure 10 and Figure 11. In this validation study, P_{EC} is represented by the unit pressure applied on the tympanic membrane (TM).

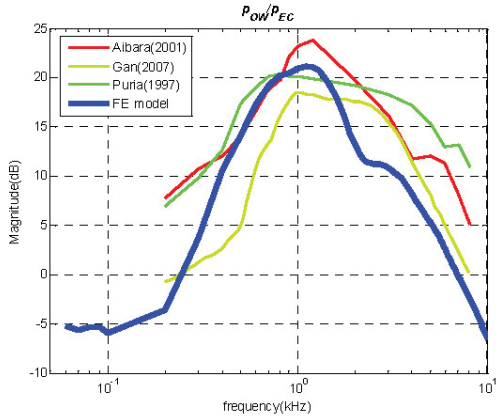

Figure 10. The ear-canal pressure magnitude, p_{EC}, to oval-window pressure, p_{OW}, middle-ear gain.

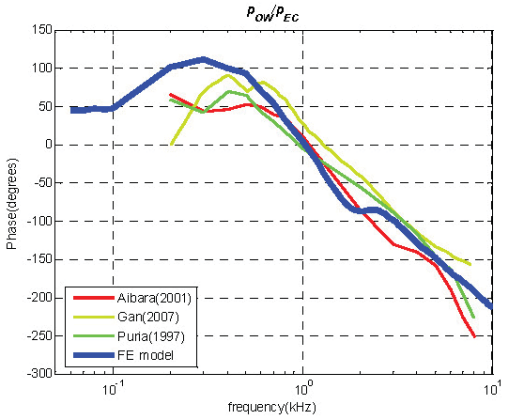

Figure 11. The ear-canal pressure phase, p_{EC}, to oval-window pressure, p_{OW}, middle-ear gain.

P_{OW}/P_{EC} is consistent with experimental data within a 5 dB range from 300Hz to 10 kHz. Figure 12 shows simulated cochlear input impedance (the ratio of the scalae pressure near the oval window (OW) to the volume velocity at the OW, P_{OW}/U_{OW}) compared with published data. Figure 12 indicates that the FE result is qualitatively consistent with published data [10,16,17,18]. However, it is observed that the simulated result is less damped or over-massed than the experimental data.

Figure 13 shows the FE-simulated Best-Frequency (BF) map along with those obtained experimentally by Greenwood [19]. The BF map indicates the peak BM vibration location among 200 measurement points along the BM as a function of frequency.

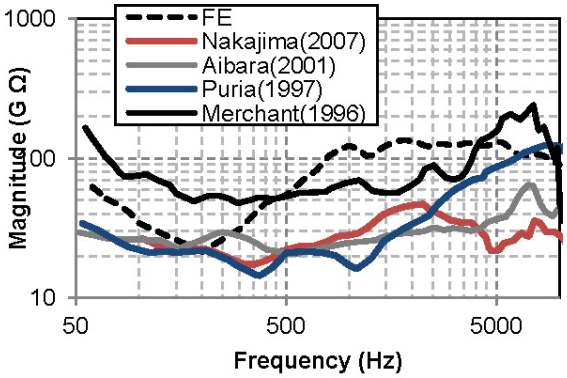

Figure 12. Cochlear input impedance, p_{OW}/U_{OW}. Magnitude in GΩ.

As shown in Figure 13, the BF map from the FE model is in agreement with the experimental data. This agreement was a result of an iterative tuning process of elastic modulus values of the BM with AC excitation.

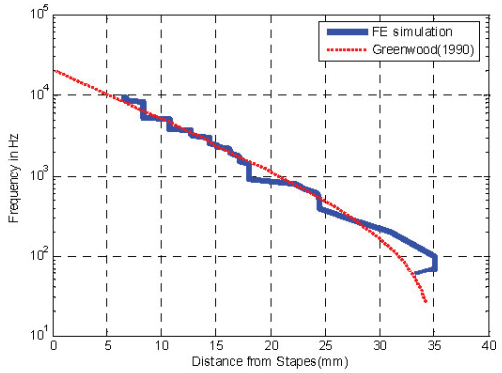

Figure 13. Simulated BF map for AC excitation along with experimental data by Greenwood [19].

Figure 14 shows the simulated and measured AC response of the BM velocity, v_{BM}, observed at a specific BM location (12 mm from the base) normalized by the stapes footplate (i.e. OW) velocity, v_{OW}. Since both BM velocity and stapes footplate velocity are vectors whose components are complex values, the calculated value with two vectors, v_{BM}/v_{OW}, cannot give any physical meaning of normalized velocities in the respect of magnitude and phase.

Therefore, the normal vectors of BM and stapes measurement points, $\mathbf{n}_{BM}$ and $\mathbf{n}_{ST}$ are obtained. It should be noted that the positive direction of each normal vector in this study is the direction from the ST to SV for the BM, and the direction from the outer ear to the inner ear for the stapes. Next, the inner product between the velocity vector and the normal vector of the measurement points is performed to obtain complex scalar values, which were the normal directional components of the velocity vector for the BM and stapes measurement points. The normalized BM velocity is calculated by the normal component of the BM velocity over the normal component of the stapes velocity. The FE result in Figure 14 shows a reasonable agreement with the measured results from the literature in terms of its overall response characteristics.

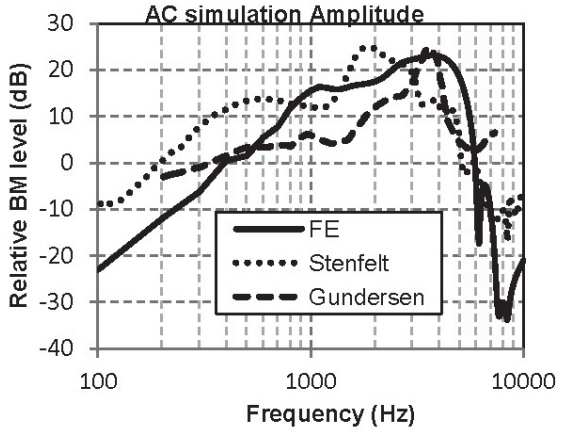

Figure 14. Auditory system model validation: (a) middle-ear pressure gain (scala vestibuli pressure over TM pressure) and (b) BM velocity in response to TM pressure normalized by stapes velocity. BM velocity was observed at 12 mm from the base for the FE result. The cadaver ear experimental data [20,21] were also obtained at a similar location on the BM.

5 VIRTUAL EXPERIMENTS

Having a FE model correlated against literature data gives a unique opportunity to further investigate the challenging questions in AC, BC and resulting pathways. The AC and BC limit difference as well as transmission paths due to the earplug are investigated.

5.1 FE Model Simulation of AC/BC Difference ("BC limit")

The difference in magnitude of AC perceived sound to BC perceived sound is referred to as the "bone conduction limit", which suggests the limit of hearing protection achievable by occluding the ear. This effect is simulated by computing the difference between the BM vibration levels, as indicated in terms of BM structural deformation for AC and BC cases, with results presented in Figure 15. The AC case is simulated by applying acoustic pressure on all external surfaces of the skull model, including the TM. This result is then compared with the BC case, where the pressure was again applied over the external skull surfaces, but not on the TM. The simulated AC/BC level difference in Figure 16 is presented to be similar to published data [1,22,23], despite the fact that the simulation lacked the flesh layer covering the skull.

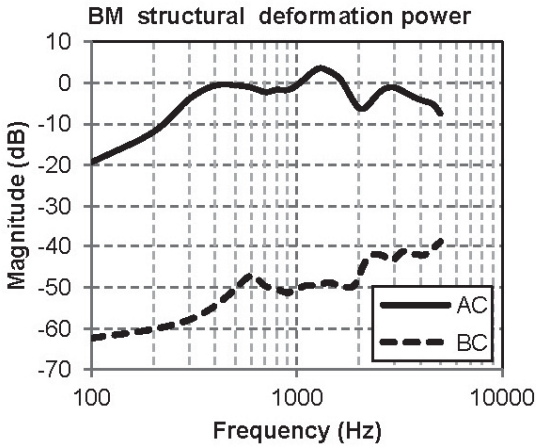

Figure 15. Simulated AC/BC sound transmission difference (i.e. BC limit) obtained with the current model: deformation power of the vibrating BM for AC and BC excitations.

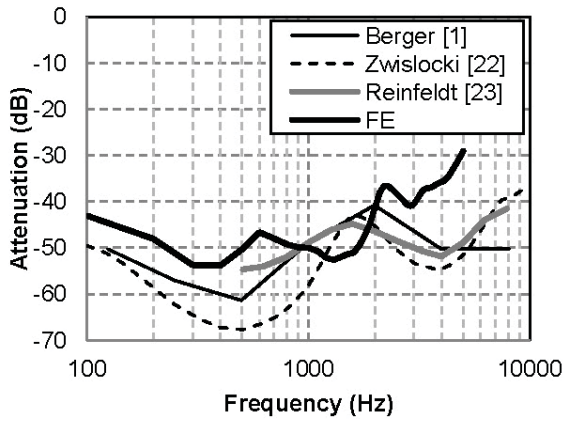

Figure 16. FE-simulated BC limit (dB difference in BM vibratory deformation power between AC and BC) compared with published data [1,22,23].

The motion of the cochlea structure as the skull undergoes BC induced vibration is observed in the FE model. This motion, which is shown in Figure 17, is qualitatively observed to be mostly comprised of rigid-body motion components (translation and rotation), with some deformational vibration components.

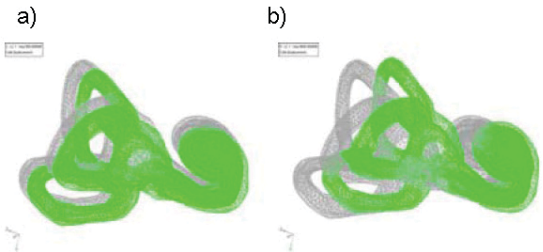

Figure 17. Snapshot images of the vibration of the cochlea realistically attached to the skull subjected to BC excitation at (a) 500 Hz and (b) 4000 Hz. Green image is the displaced state, and the gray image is the undeformed state. (Not to scale)

5.2 Sound transmission path analysis

The paths of sound transmission from the noise source via the flesh/plug system to the TM are investigated. Figure 18 below shows a conceptual diagram of the sound transmission paths for an ear fitted with an earplug. The external sound pressure acts on both the surface of the circumaural flesh, A, and the back surface of the plug, B, which in turn vibrates the tied plug/flesh system. The displacement degrees of freedom of the flesh and plug are mutually coupled, as indicated by the bi-directional arrow C in the diagram. The occluded acoustic pressure in the ear canal is generated through surface vibrations of the tip of the earplug (E), as well as the flesh (D) lining the ear-canal wall.

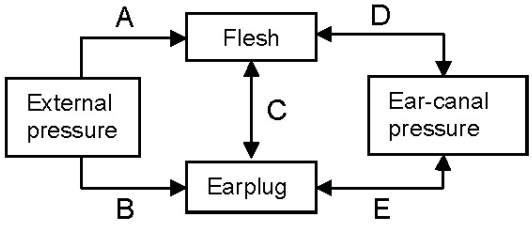

Figure 18. The transmission path diagram

The relative strength of each of these transmission paths can be analyzed in the FE model by selectively eliminating the coupling interfaces, which are labeled in Figure 18 as components A through E, and examining the resulting impact on TM pressure. Figure 19 below shows changes in resulting TM pressure due to different coupling conditions. The 0 dB line is the baseline case with all coupling interfaces intact. The earplug insertion depth used in these analyses is representative of a typical deep-insert earplug, whose tip is located near the bony canal entrance.

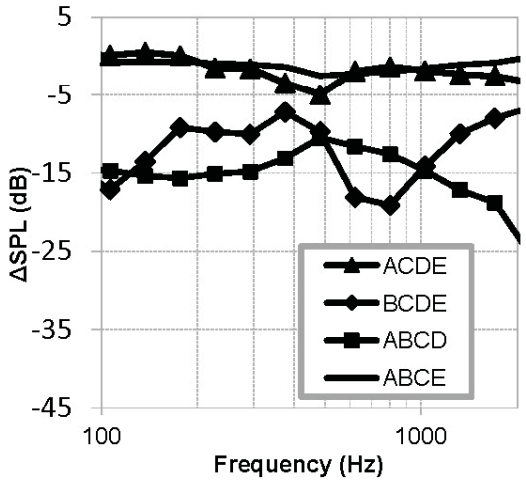

Figure 19. Changes in TM acoustic pressure (ΔSPL) by selectively de-activating coupling interfaces. The dB changes are relative to the baseline case where all interfaces are active. For example, ACDE stands for the case where the interface B is deactivated while other interfaces are intact.

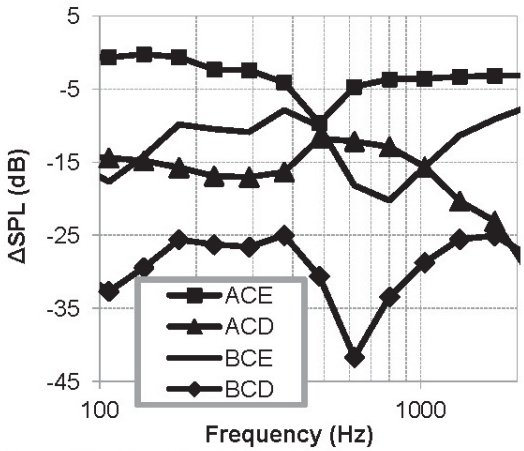

Figure 20. ΔSPL for different pathways

Figure 19 shows that effectively eliminating interface B (case ACDE), does not result in significant reductions in TM pressure as compared with eliminating interface A (case BCDE). This suggests that the relative contribution of the sound-to-flesh coupling is larger than that of the sound-to-plug coupling. This is expected considering that the area of the flesh where the incident sound acts upon is significantly larger than that of the plug. From the ABCD and ABCE results in Figure 19, it can be deduced that the main source generating TM pressure can be attributed to the vibrating surface of the earplug tip rather than that of the ear canal flesh. Again, this is expected considering that the deep-insert earplug constrains large portions of the thicker ear canal flesh, and terminates near the body canal entrance of the bony ear canal where thinner flesh layers have minimal contribution on occluded air pressure generation. However, it should be noted that the relative contribution of the flesh wall to the TM pressure would increase if the plug insertion depth is reduced, which exposes more of the thicker vibrating flesh wall. Further analysis is needed in conjunction with the insertion depth analysis described in the previous section. Figure 20 shows cases where two coupling interfaces (one outer and one inner) are deactivated. The results indicate that the strongest path is ACE (outer pressure → flesh outer surface → plug → TM pressure) while the weakest is BCD (outer pressure → plug outer surface → canal wall flesh → TM pressure).

6 CONCLUSIONS

A general framework for developing detailed biomedical numerical models for AC and BC pathways, including ear insert HPD in high noise environments is presented. Starting with *in vivo* CT scanning to obtain an individual's ear canal, then using microCT scanning to obtain middle ear and cochlea geometries of generalized cadaver subjects, geometrical components of the biomedical FE are developed. The material properties of the components are initially acquired from literature information. Using several responses taken from published data for each component, initial material properties are tuned iteratively to exhibit consistent response. It is shown that the FE model may be simplified based on the frequency of interest. For example, the skull has a natural frequency of 1 kHz, therefore simplification can be obtained by imposing proper boundary conditions up to 1kHz instead of including the full skull in the FE model, which is effectively inactive in this frequency region. The completed and validated FE model is used to answer many challenging questions plaguing the hearing protection community. In this study, the BC limit and noise transmission pathways of flesh/plug systems are investigated. It is shown that there exists 5dB error in BC limit calculations of the FE model as compared to published experimental data. Considering the variability of human anatomical measurements and material properties, the obtained results are considered to be in agreement with literature results. Obtaining validated FE models enables the future development of advanced hearing protection systems, as well as novel hearing protection evaluation systems that can provide experimentally correlated psychoacoustic noise attenuation [24]. Explained FE model methodology and techniques may be further used to simulate the effects of blast related impulse noise on human auditory mechanisms and the brain.

7 ACKNOWLEDGEMENT

Research was supported by the Air Force Office of Scientific Research (AFOSR) under STTR funding (Contract NO: FA9550-06-C-0039) and grant DC 007910 from the NIDCD of NIH. Continuing work is currently being funded by NAVAIR SBIR funding (Contract No. N68335-10-C-0430).

REFERENCES

1 Berger, Elliott H., Kieper, Ronald W., and Gauger, Dan. Hearing protection: Surpassing the limits to attenuation imposed by the bone-conduction pathways. *J. Acoust. Soc. Am.*, 114, 4 (October 2003), 1955-1967.

2 Koike, T., Wada, H., and Kobayashi, T. Modeling the human middle ear using the finite-element method. *J. Acousti. Soc. Am.*, 111, 3 (2002), 1306-1317.

3 Gan, R. Z., Feng, B, and Sun, Q. Three-dimensional Finite Element Modeling of Human Ear for Sound Transmission. *Annals of Biomedical Engineering*, 32, 6 (2004), 847-859.

4 Steele, C.R. and Taber, L.A. Comparison of WKB calculations and experimental results for three-dimensional cochlear models. *J. Acoust. Soc. Am.*, 65 (1979), 1007-1018.

5 Pathasarathi, A.A., Grosh, K, and Nuttall, A.L. Three-dimensional numerical modeling for global cochlear dynamics. *J. Acousti. Soc. Am.*, 107, 1 (2000), 474-485.

6 Stenfelt, Stefan. Acoustic and physiologic aspects of bone conduction hearing. *Advances in oto-rhino-laryngology*, 71 (2011), 10-21.

7 von Békésy, G. Vibration of the head in a sound field and its role in hearing by bone conduction. *J. Acousti. Soc. Am.*, 20, 6 (1948), 749-760.

8 Stenfelt, S. Transmission properties of bone conducted sound: measurements in cadaver heads. *J. Acousti. Soc. Am.*, 118, 4 (2005), 2373-2391.

9 Stenfelt, S. Vibration characteristics of bone conducted sound in vitro. *J. Acousti. Soc. Am.*, 107, 1 (2000), 422-431.

10 Aibara, R., Welsh, J.T., Puria, S., and Goode, R.L. Human middle-ear sound transfer function and cochlear input impedance. *Hearing Restoration*, 152 (2001), 100-109.

11 Lee, C., Chen, P., Lee, W., Chen, J., and Liu, T. Three dimensional reconstruction and modeling of middle ear biomechanics by high-resolution computed tomography and finite element analysis. *Laryngoscope* , 116 (2006), 711-716.

12 Lee, C.F., Hsu, L.P., Chen, P.R., Chou, Y.F., Chen, J.H., and Liu, T.C. Biomechanical modeling and design optimization of cartilage myringoplasty using finite element analysis. *Audiology & Neuro-Otology*, 11, 6 (2006), 380-388.

13 Homma, K. *Advanced Finite Element Model Development for Characterization and Mitigation of Bone Conducted Sound Transmission in High Noise Environment.* STTR Phase II Contract Number FA9550-07-C-0088, 2010.

14 Gan, R.Z., Reeves, B.P., and Wang, X. Modeling of Sound Transmission from Ear Canal to Cochlea. *Annals of Biomedical Engineering*, 32 (2007), 847–859.

15 Homma, K., Du, Y., Shimizu, Y., and Puria, S. Ossicular resonance modes of the human middle ear for bone and air conduction. *J. Acoust. Soc. Am.*, 125 (2009), 968-979.

16 Merchant, S.N., Ravicz, M.E., and Rosowski, J.J. Acoustic input impedance of the stapes and cochlea in human temporal bones (1996).

17 Puria, S., Peake, W.T., and Rosowski, J.J. Sound-pressure measurements in the cochlea vestibule of human cadaver ears. *J. Acoust. Soc. Am.*, 101 (1997), 2754-2770.

18 Nakajima et al., H.H. Clinical investigation and mechanism of air-bone gaps in large vestibular aqueduct syndrome. *The Annals of Otology, Rhinology, and Laryngology*, 116, 7 (2007), 532-541.

19 Greenwood, D.D. A cochlear frequency-position function for several species-29 years later. *J Acoust Soc Am*, 87, 6 (1990), 2592–2605.

20 Stenfelt, S., Puria, S., Hato, N., and and Goode, R.L. Basilar membrane and osseous spiral lamina motion in human cadavers with air and bone conduction stimuli.. *Hearing Restoration*, 181 (2003), 131-143.

21 Gunderson, T., Skarstein, O., and Sikkeland, T. A study of the vibration of the basilar membrane in human temporal bone preparations by the use of the Mössbauer effect. *Acta Otolaryngol.*, 86 (1978), 225-232.

22 Zwislocki, J. In search of the bone-conduction threshold in a free sound field. *J. Acoust. Soc. Am.*, 29, 7 (1957), 795-804.

23 Reinfeldt, S, Stenfelt, S., and Håkansson, B. Examination of bone-conducted transmission from sound field excitation measured by thresholds, ear-canal sound pressure, and skull vibrations. *J. Acoust. Soc. Am.*, 121, 3 (2007), 1576-1587.

24 Schank, K., *Development of Advanced Hearing Protection Evaluation System.* SBIR, Contract No. W911QX-10-C-0080.